RESEARCH ARTICLE

Reflective Metasurface With Steered OAM Beams for THz Communications

ALI ALI, (Graduate Student Member, IEEE), **MOHSEN KHALILY**, (Senior Member, IEEE),
DEMOS SERGHIOU, (Student Member, IEEE),
AND RAHIM TAFAZOLLI, (Senior Member, IEEE)

Home of 5G and 6G Innovation Centres, Institute for Communication Systems (ICS), University of Surrey, GU2 7XH Guildford, U.K.

Corresponding author: Mohsen Khalily (m.khalily@surrey.ac.uk)

ABSTRACT The abundant spectrum resources and low beam divergence of the terahertz (THz) band, can be combined with the orthogonal propagation property of orbital angular momentum (OAM) beams to multi-fold the capacity of wireless communication systems. Here, a reflective metasurface (RMTS) is utilized to enhance the coverage of the high gain THz OAM beams by enabling the non-line-of-sight (NLoS) component by reshaping the planar wavefront of the incident wave into the helical wavefront, so that it is re-directed towards the direction of interest. This can contribute to alleviating the concern of the small aperture size, since improving the channel capacity can be achieved at the low spectrum blocks of the THz band (larger aperture size). For validation, three 90×90 mm RMTSs are simulated, fabricated, and tested in the frequency range 90-110 GHz, to re-direct single and dual OAM beams towards the desired location.

INDEX TERMS Sixth-generation (6G), orbital angular momentum (OAM), reflective metasurface (RMTS), terahertz (THz).

I. INTRODUCTION

For a long time, terahertz (THz) applications were confined to imaging and sensing as pertinent to the scarcity of high-efficiency THz devices [1]. However, the rapid development of THz technologies has attracted attention to the THz gap (between 100 GHz and 10 THz) to be used in several applications associated with security, astronomical observation, and localization [2], [3], [4]. Nevertheless, the growth of the world's hunger for higher data rates and low latency wireless communications will deplete the available frequency resources [5], which has motivated researchers to resort to the THz regime. To integrate delay-sensitive and data-demanding applications, driving up the channel frequency to the THz regime can be embraced to satisfy the demand for higher capacities [6]. Thus, employing THz spectrum blocks will enable operators to improve wireless communications and provide a plethora of non-communication applications.

In addition to utilizing higher frequencies, the spatial distribution of propagated waves can be employed as a

new modulation procedure to enhance the system's throughput. For example, orbital angular momentum (OAM) beams can improve channel capacity and spectral efficiency for short-range THz communications [7]. The orthogonality among different OAM modes enables exchanging of data simultaneously through several streams at the same frequency, compared to sending a single beam in traditional antennas. This screw dislocation of phase can be expressed mathematically by $e^{jl\varphi}$, where l denotes the mode's number or the changes of the wavefront around the intensity null and φ represents the azimuthal angle [8], [9]. By that, no additional resources, such as power, time, and frequency, will be required to deliver services to users [10]. Employing OAM beams means that a new generation of transceivers will begin, since these beams depend on the angular momentum compared to the linear momentum of traditional devices, which is restricted to one-dimensional motion.

Generating THz OAM beams can bring multi-fold benefits related to improving the bandwidth, channel capacity, and spectral efficiency. That returns to the vast bandwidth of the THz band and the additional degree of freedom provided by the OAM beams. Not to forget that the beam divergence

decreases at short wavelengths, so the OAM beam divergence reduces at higher frequencies [11]. Adding to that, the short wavelength of THz frequencies will minimize the size of structures, so hundreds of antennas can be packed together, which contributes to reducing the divergence problem of OAM waves as well. Besides, this integration can reinforce both security and integrated sensing and communications.

Despite the promising solution provided by THz OAM waves, the high directivity of waves can lead to poor network coverage in the absence of the line-of-sight (LoS) component. The blockage of THz links would make them highly susceptible to attacks, even in short-range communications [12]. That returns to poor diffraction and scattering abilities of THz waves as well as being exposed to atmospheric attenuation. Accordingly, coverage enhancement should be given high priority. On the other hand, THz waves suffer from a lack of strong electromagnetic (EM) response from naturally occurring materials [13]. Engineered metasurfaces are a potential solution to enable the exotic EM properties and develop efficient and compact THz components. One of the advantages of using metasurfaces is manipulating the anomalous reflection of the arbitrary incident EM wavefront by two-dimensional (2D) metamaterials [14], [15].

In the latest report of the international telecommunication union (ITU), the RIS and OAM technologies at THz frequencies have been proposed as promising solutions to realize a full utilization of the spatial dimensions and enhance the performance of antennas [16]. Intelligent reflecting surface (IRS) has drawn the attention of the research society since it can play a critical role in the transition towards highly efficient and coverage-enhanced networks [17]. The developed networks can deliver high-quality-of-service (QoS) to loads of subscribers by sensing the environment, recycling existing radio waves, and enabling non-line-of-sight (NLoS) communications [18], [19]. The integration between RIS and OAM at THz frequencies can solve the limited bandwidth issue of RIS structures, reduce the divergence of OAM, and improve spectral efficiency. Moreover, the fabrication complexity at the high THz spectrum blocks can be alleviated by employing low THz frequencies. Thus, high spectral efficiency can be maintained at the desired frequency bands.

The rest of the paper is organized as follows: Section II discusses the motivation and contributions of our work. Afterwards, the design procedures of the unit cell and RMTSs for single- and dual-steered OAM beams are examined in Section III. Following that, simulation and experimental results are presented and compared in Section IV. Finally, Section V summarizes the contents of this paper.

II. MOTIVATION AND CONTRIBUTIONS

Frequencies at low spectrum blocks of the THz band (below 300 GHz) are not exposed to high levels of molecular absorption, allowing for short-range communications up to a few hundred meters [20]. Accordingly, it would be doable
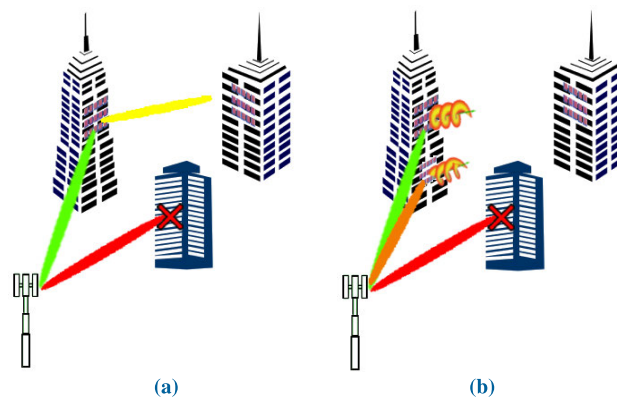
FIGURE 1. RMTS-assisted wireless communications to enable NLoS transmission for short-range THz communications. (a) traditional beams, (b) OAM beams.

to operate THz IRSs to bypass the obstacles between the base stations (BSs) and users to achieve NLoS communications via short-distance links. Loads of advantages can be gained by utilizing IRSs, associated with introducing low-profile and power-efficient antennas that make them environment-friendly structures with the capability to perform full-band transmission.

The system's throughput can be enhanced even more by increasing the spectral efficiency to obtain the maximum utilization of the available bandwidth. The inherent orthogonality among OAM modes can be operated to simultaneously split data between multiple data modes for the same frequency. The generation of helical waves has been addressed in the literature by various structures of different features. The majority of the state-of-the-art designs are restricted to producing a single OAM state [21], [22], or are not feasible to be fabricated in the immediate term [23]. Nevertheless, many successful designs introduced multi-OAM states at the expense of increasing the system's complexity, price, and beam divergence through concentric uniform circular arrays (UCAs) [24]. The capability of the THz-IRS structure to flexibly control the phase of incident EM waves promotes employing this low-cost and highly reliable solution to generate different OAM modes. This paper introduces a reflective metasurface (RMTS) not only to enable NLoS communications but also to highlight the capability of these structures to convert the planar wavefront of the impinged beam into a helical wavefront (see Fig. 1). The large number of scatterers with a controllable phase of RIS can be utilised to overcome the disadvantages of traditional methods to generate OAM beams [10]. Here, directed beams with unique OAM modes are produced by three RMTSs in the band between 90 and 110 GHz. At this range of frequencies, reduced modal power coupling among the modes and less distortion occurs [25]. The power-free THz-RMTS can provide good coverage, enhanced bandwidth, high spectral efficiency, and low-cost secured communications. To the best of the authors' knowledge, the proposed design is the first fabricated and tested OAM-based THz RMTS.

III. RMTS DESIGN

This section reviews the design process and EM concepts pertinent to the RMTS to generate directed OAM beams. A comparison between two unit cells will be introduced first, followed by discussing and rendering the required phase distributions for single and dual OAM beams.

A. UNIT CELL

The phasing scatterers are prone to patterning, fabrication, or even analysis approximation errors. The quantization error can happen due to the low accuracy of the fabrication process, where choosing the wrong dimension (or rotation) of the selected elements will cause a difference between the desired and quantized phases. Besides, the unit cell should provide a complete phase cycle (360°) so that the closest quantized phase can be realized. However, to maintain periodicity, the dimensions of unit cells should be small relative to the wavelength. Unit cells of less than ($\lambda/2$) are usually employed to reduce the phase quantization error and achieve a smoother phase variation. The phase error can be expressed by:

$$err\,(m,n) = \left| \psi_{co-pol}^{d}\,(m,n) - \psi_{co-pol}^{r}\,(m,n) \right| \quad (1)$$

where $\psi_{co-pol}^{d}\,(m,n)$ represents the needed reflection phase of the mn^{th} unit cell and $\psi_{co-pol}^{r}\,(m,n)$ is the realized co-polar reflection phase [26].

Nevertheless, the transition towards higher frequencies raises the difficulty of fabrication. Accordingly, the trade-off between the phase error and fabrication complexity should be thoroughly considered. Multi-layer or stacked unit cells can be utilized as an alternative solution since they improve the phase range and reduce the lattice size [27]. Furthermore, lattice and scatterer can be square, rectangular or hexagonal shaped. For this reason, the reflection coefficients of square and hexagonal-shaped patches were investigated here as functions of the width w, as shown in Figs. 2(a) and (b). It is clear in Figs. 2(c) and (d), the hexagonal lattice delivers better performance for the reflection phase and magnitude compared to the coefficients of the square element. Knowing that the hexagonal lattice offers good performance in respect of dispersion isotropy and polarization sensitivity [28].

Accordingly, the element and lattice of the proposed design are selected to be hexagonal, as displayed in Fig. 2(a). The parameters of the proposed scatterer are optimized to achieve an adequate reflection phase range and keep the reflection magnitude close to 0 dB [29]. Adopting hexagonal elements of $\lambda/2.5$ at 110 GHz ($\lambda/3$ at 90 GHz) with a single copper patch as a variable to compensate for the phase can bring loads of benefits, since improved control can be achieved by reducing the empty spaces among elements. Moreover, the fabrication accuracy increases when a single solid patch is distributed over the surface.

The configuration of the proposed unit cell is depicted in Fig. 2(a). It is a wideband stacked element with a Rogers RT5880 substrate of $h_1 = h_2 = 0.127$ mm thickness. The hexagons' diameter is around $s = 1.1$ mm, whereas the
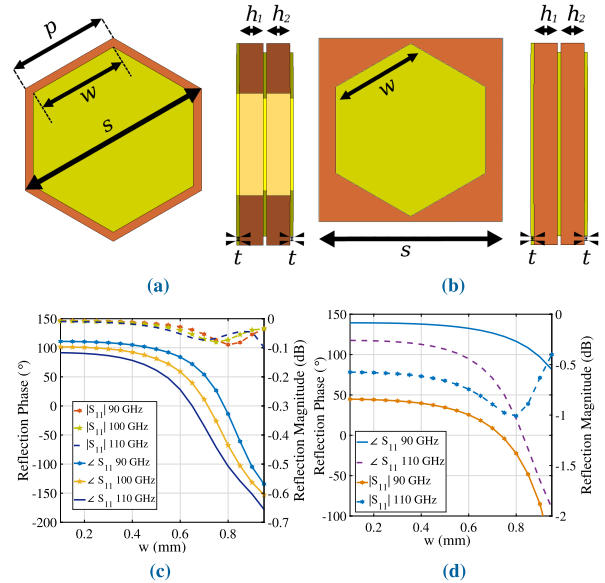
FIGURE 2. Comparison between hexagonal and square shaped elements in the frequency range 90- 110 GHz. (a) hexagonal element geometries, (b) square element geometries, (c) hexagonal element reflection coefficients, (d) square element reflection coefficients.

parameter w varies between 0.1 to 1 mm to guarantee a phase range of around 270° at the desired bandwidth. The achieved phase range can be considered sufficient for the proposed RMTSs since they will be illuminated by plane waves. That can be observed in the obtained phase distributions, as we will see in the next section. Fig. 2(c) illustrates the reflection phase and magnitude responses as functions of w in the frequency range between 90 and 110 GHz. Results were obtained by CST Studio Suite with the periodic boundary condition and Floquet excitation.

B. ORBITAL ANGULAR MOMENTUM

When a plane wave impinges the metasurface, it induces surface currents on the RMTS. By manipulating the phase of each element, the received beam can be reshaped and reflected. This modulation usually mimics the shape of the desired beam. For example, the phase distribution could be made of concentric circles to generate the spherical wavefront of pencil beams. Again, that can be utilized to produce vortex beams carrying OAM where the geometries should follow a helical phase distribution of $e^{j.l.\varphi}$ (l refers to the mode number and φ represents the azimuthal angle). To obtain a vortex with a specific mode l for metasurfaces with a feeder as in reflectarray antennas (RAs), each mn^{th} element should reflect a phase of [30]:

$$\psi_{mn} = k_0 \left(R_{mn} - \vec{r}_{mn}.\hat{u}_b \right) + l \times \arctan\,(y_n/x_m) + \psi_0 \quad (2)$$

where k_0 refers to the free space wave number, and the distance between the desired scatterer and the feeding horn is denoted by R_{mn}. $\hat{u}_b$ is the beam direction, $\vec{r}_{mn}$ stands for its vector, the point (x_m, y_n) represents the element's position, and ψ_0 refers to a constant phase.
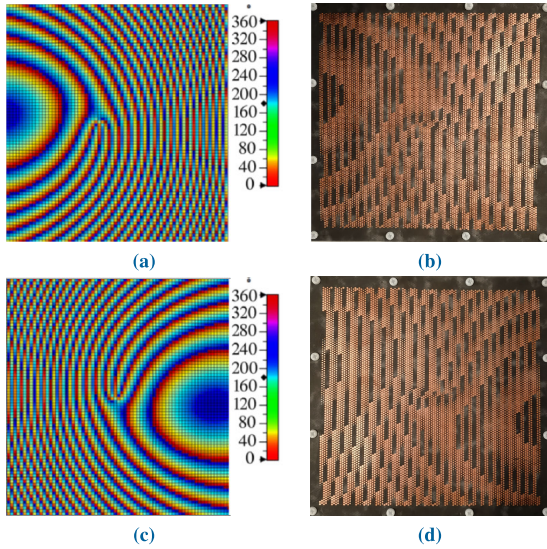
FIGURE 3. Phase patterns and associated layouts of RMTSs. (a) spiral phase distribution for $\theta = -45°$, (b) layout, (c) spiral phase distribution for $\theta = +45°$, (d) layout.

Therefore, to change the beam direction, $\hat{u}_b$ and $\vec{r}_{mn}$ should be configured based on the elevation and azimuth angles θ and φ, respectively.

1) SINGLE OAM BEAM DIRECTED TOWARDS A DESIRED ANGLE

It can be noticed that the main difference between RA and RMTS is the source of the incident wave. An RA usually would have a feeder, so the distance between the RA and feeder, called focal length (F), determines the phase distribution to compensate for the potential reception delay among the distributed elements. Nonetheless, it is assumed that the RMTS will be illuminated by a plane wave [31]. For simplicity, the phase distribution of the RMTS can be acquired by substituting the distance between the transmitter of the plane wavefront and metasurface (D) in (2), so the phase can be obtained by:

$$\psi_{mn} = k\left(D - \sin\theta \cdot (x_m \cdot \cos\varphi + y_n \cdot \sin\varphi)\right) + l \times \psi_t + \psi_0 \tag{3}$$

where θ and φ can be used to change the course of the beam towards the required direction.

Fig. 3 demonstrates the calculated phase distributions and the associated layouts for two different RMTSs with directed beams ($\theta = -45°$, $\varphi = 0°$) and ($\theta = -45°$, $\varphi = 0°$) of the third OAM mode between 90 and 110 GHz. Figs. 3(a) and (c) depict the phase obtained for each element based on (3) considering $D = 350$ mm and the size of each RMTS equals 90×90 mm. Accordingly, Figs. 3(b) and (d) show the fabricated metasurfaces.

2) DUAL OFF-CENTRED OAM BEAMS DIRECTED TOWARDS DESIRED ANGLES

The conventional routines to produce multiple beams depend mainly on superposition or holography [32], [33]. The phase
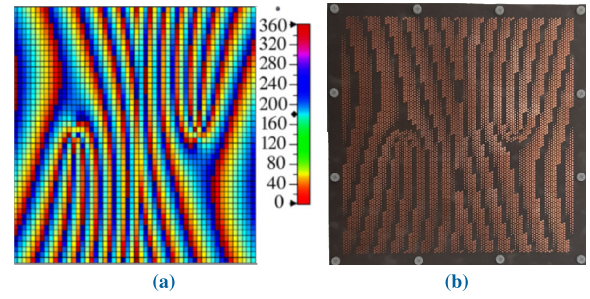
FIGURE 4. Phase pattern and associated layout of the RMTS. (a) spiral phase distribution for $\theta = \pm25°$, (b) layout.

distribution can be obtained through the sum of phase sets of multiple beams, so it is called the superposition technique. Therefore, the desired waves are radiated from different discontinuities on the surface. Whereas in holographic structures, the interference pattern is described by the surface impedance, which should represent the phase variation of a reference wave and the phase projection of an objective wave. The main drawbacks of the previously mentioned methods are related to the high sidelobes and challenging requirements for manufacturing at high frequencies [34].

The needed phase distribution to generate dual-directed OAM beams by the proposed RMTS can be obtained by modifying the formula introduced for RAs in [23]. In principle, all the forms of generating OAM beams create delay paths for the incident wave to re-generate vortices. By making the phase delay lines follow a fork shape, the circular paths can be converted into several branches, as shown in Fig. 4(a). Therefore, the main contribution of the phase will be near the fork lines, whereas the ambient lines will work on replicating the signal. Accordingly, only that part is considered in this work. Besides, elements with a size of around $\lambda/2.5$ at 110 GHz were chosen for all the studied RMTSs of 90×90 mm to achieve smoother OAM phase variation. Thus, the phase distribution of both beams is accommodated in a single RMTS. Producing dual beams requires new centres $O_k(x_{m_t}, y_{n_t})$ at which waves would be radiated, so the phase delay distribution of each beam can be obtained based on its position in the metasurface as follows [23]:

$$\psi_t = \arctan\left(((y_o - d/2) - y_{n_t})/((x_o \pm d/4) - x_{m_t})\right) \tag{4}$$

where $t = 1, 2, 3, ..etc$ indicates the number of beams. d denotes the length of the RMTS side, and $O(x_o, y_o)$ is the main centre point of the metasurface.

The total phase distribution, shown in Fig. 4(a), is computed by substituting (4) in (3) as follows:

$$\begin{aligned}\psi_{mn} = {} &k_0\left(D - \sin\theta \cdot (x_{m_t} \cdot \cos\varphi + y_{n_t} \cdot \sin\varphi)\right) + l_t \\ &\times \arctan\left(((y_o - d/2) - y_{n_t})/((x_o \pm d/4) - x_{m_t})\right) \\ &+ \psi_0\end{aligned} \tag{5}$$

Accordingly, the prototype of the proposed RMTS with dual OAM beams steered towards $\theta = -25°$ & $\varphi = 0°$ and $\theta = +25°$ & $\varphi = 0°$ of the fourth mode is depicted in Fig. 4(b). The RMTS contains 82×82 stacked unit cells
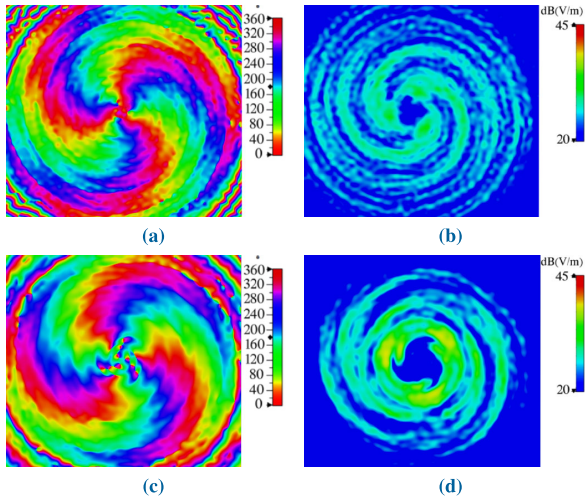
FIGURE 5. Simulation results of RMTSs with single directed OAM beams of the third mode at 90 GHz. (a) E-field phase distribution for $\theta = -45°$, (b) E-field magnitude distribution for $\theta = -45°$, (c) E-field phase distribution for $\theta = 45°$, (d) E-field magnitude distribution for $\theta = 45°$.

FIGURE 6. Simulation results of the RMTS with dual directed OAM beams at 90 GHz. (a) E-field phase distribution over the surface, (b) E-field magnitude distribution over the surface, (c) E-field phase distribution for $\theta = \pm 25°$, (d) E-field magnitude distribution for $\theta = \pm 25°$.

and an overall size of 90 × 90 mm. It should be noted that prototypes were fabricated with the low-cost printed circuit board (PCB) technique.

IV. SIMULATION AND EXPERIMENTAL RESULTS
In this section, the design principle of the presented RMTSs in the range 90-110 GHz is validated through simulation and measurement results as follows:

A. SIMULATION RESULTS
Numerical simulations were conducted to demonstrate the performance of the RMTSs in CST Microwave Studio Suite for single and dual directed OAM beams at 90 and 110 GHz. A plane wave tool is used to illuminate the metasurface. The phase and magnitude distributions of the electric field (E-field) of directed OAM beams can be detected by rotating the observation cross-section. So, it would be perpendicular to the propagation direction. The needed rotation can be obtained by using transformation matrices by transforming the cross-section with an angle of ±45 around the x-axis. Figs. 5(a) and (c) exhibit the E-field's spiral distributions for $\theta = -45°$ and $\theta = 45°$, respectively. On the other hand, Figs. 5(b) and (d) demonstrate the intensity null at the centre of the magnitude distributions of the E-field.

The E-field properties of the RMTS with dual directed OAM beams can be obtained by following similar steps. Taking into account that the cross-section needs to be transformed two times to observe the E-field of each beam (with an angle of ±25 around the x-axis). The phase delay lines are shown in Figs. 6(a) and (b) for the phase and magnitude, obtained by a cross-section parallel to the RMTS. On the other hand, the E-field phase distribution of the fourth OAM mode is indicated in Fig. 6(c) with spiral lines. Besides that, the energy gap can be seen in the E-field magnitude distribution Fig. 6(d).
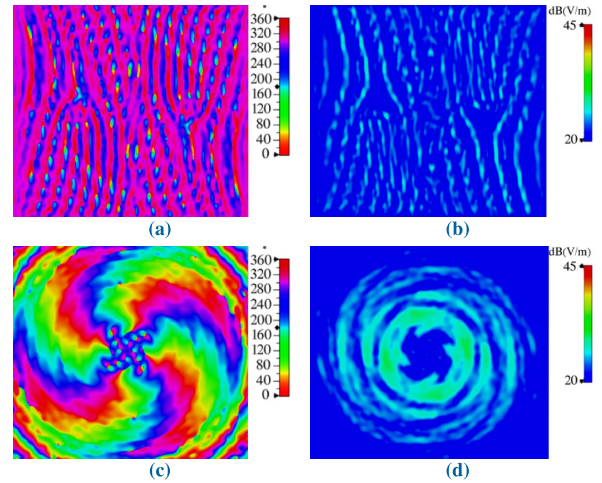
The corresponding far field radiation patterns for single OAM beams are displayed in Figs. 7(a) and (b) and Figs. 7(g) and (h) at 90 and 110 GHz, respectively. The simulation results show the waves' rotation around zero energy intensity. That matches the properties of beams carrying OAM of the third mode for the designed RMTSs. Further, producing dual OAM beams can be confirmed by observing the far field radiation patterns depicted in Figs. 7(c) and (i) at 90 and 110 GHz, respectively. Thus, it can be proved by simulations that single and dual directed OAM beams were successfully generated with $l = 3$ and $l = 4$.

Here, a spectral analysis of the Fourier transform is employed to assess the purity of the generated OAM beams. The sampling phase $F(\phi)$ is extracted along a circle, so the Fourier relationship can be written as [35]:

$$F(\phi) = \sum_l a_l e^{jl\phi} \tag{6}$$

$$a_l = \frac{1}{2\pi} \int_0^{2\pi} F(\phi) e^{-jl\phi} d\phi \tag{7}$$

where a_l is the OAM spectrum.

Figs. 7(d) and (e) and Figs. 7(j) and (k) illustrate the purity of third OAM modes for RMTS with $\theta = -45°$ and $\theta = 45°$ at 90 and 110 GHz, respectively. In addition, the purity figures for the fourth OAM mode, generated by the dual beam RMTS with $\theta = \pm 25°$, are shown in Figs. 7(f) and (l). The dominant $l = 3$ and $l = 4$ OAM modes can be evidently observed in the results for the selected carrier frequencies.

B. EXPERIMENTAL RESULTS
The measurement results of the proposed RMTSs were obtained through TeraScan 1550 manufactured by TOPTICA. The device configuration covers frequencies between 90 GHz and 2.7 THz. It is composed of distributed feedback (DFB) laser diodes with gallium arsenide (GaAs) or indium gallium arsenide (InGaAs) photo-mixes. The beam-width of
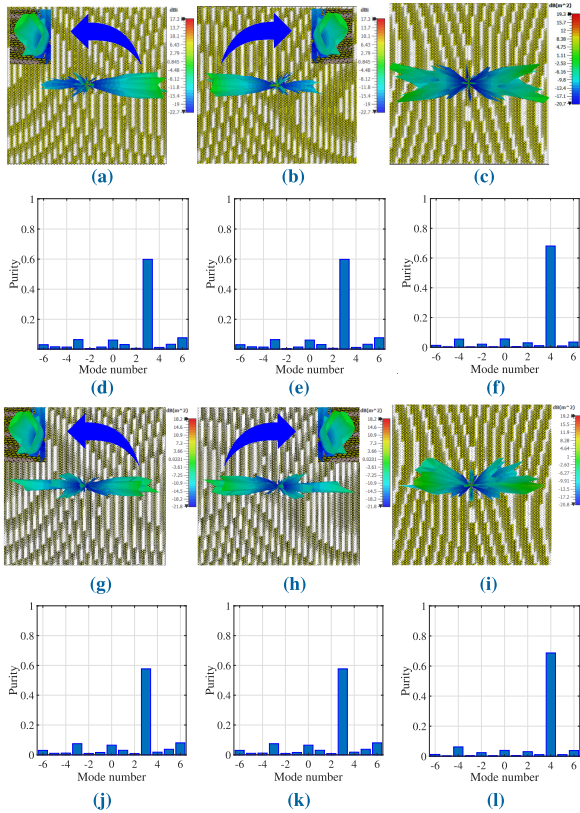
FIGURE 7. Radiation patterns and purity figures of the proposed RMTSs at 90 and 110 GHz. (a) $\theta = -45°$ at 90 GHz, (b) $\theta = 45°$ at 90 GHz, (c) $\theta = \pm 25°$ at 90 GHz, (d) $l = 3$ and $\theta = -45°$ at 90 GHz, (e) $l = 3$ and $\theta = 45°$ at 90 GHz, (f) $l = 4$ and $\theta = \pm 25°$ at 90 GHz, (g) $\theta = -45°$ at 110 GHz, (h) $\theta = 45°$ at 110 GHz, (i) $\theta = \pm 25°$ at 110 GHz, (j) $l = 3$ and $\theta = -45°$ at 110 GHz, (k) $l = 3$ and $\theta = 45°$ at 110 GHz, (l) $l = 4$ and $\theta = \pm 25°$ at 110 GHz.

FIGURE 8. System configurations and comparisons between simulation and experimental results. (a) a single OAM beam directed towards $\theta = -45°$ and $l = 3$ at 90 GHz, (b) $\theta = -45°$ and $l = 3$ at 90 GHz, (c) a single OAM beam directed towards $\theta = 45°$ and $l = 3$ at 90 GHz, (d) $\theta = 45°$ and $l = 3$ at 90 GHz, (e) dual OAM beams directed towards $\theta = \pm 25°$ and $l = 4$ at 90 GHz, (f) $\theta = \pm 25°$ and $l = 4$ at 90 GHz.
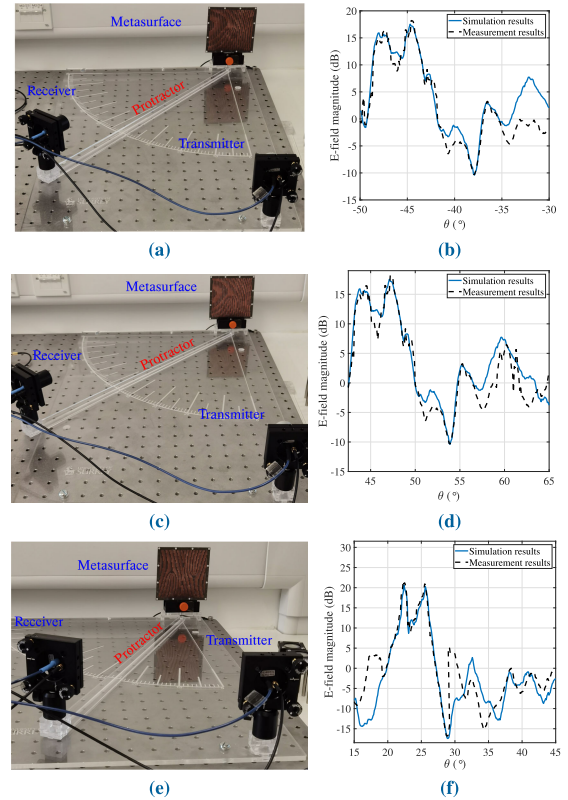
the transmitter α is close to $10°$ at the specified range of frequencies. Thus, the distance (di) between the emitter and the surface can be given by:

$$di = \frac{L}{2 \tan (\alpha/2))} \tag{8}$$

where L denotes the width of the RMTS.

Thus, to illuminate a 90×90 mm metasurface, di should be around 51.4 cm for the range between 90 and 110 GHz. Since the OAM beams are steered towards different angles, a platform with a protractor was needed to accurately attain the required rotations.

Figs. 8(a), (c), and (e) illustrate the system configuration of the discussed RMTSs. The first configuration started by rotating the arm to be located at $45°$ as shown in Fig. 8(a). The measured amplitude of the E-field is over 17.5 dB, as demonstrated in Fig. 8(b) (black dashed plot). Since only a half protractor is supported by the platform, to do the measurement for the second RMTS, we rotated it around its z-axis by $180°$ to direct the beam towards the receiver as portrayed in Fig. 8(c). Accordingly, around 16.5 dB is achieved for the measured amplitude of the E-field pattern, displayed in Fig. 8(d). The last setup was performed twice to measure the dual directed OAM beams at 90 GHz. In the first time,

the arm was located at $-25°$ to measure the reflected OAM beam. In the following measurement, the RMTS was rotated around its axis to direct the $25°$ OAM beam to the receiver, as Fig. 8(e) exhibits. Fig. 8(f) confirms the generation of OAM through the observed singularity in the magnitude distribution of the measured E-field.

At the same time, Figs. 8(b), (d), and (f) compare the simulated results (continuous blue lines) and measured results (dashed black lines). The good alignment between these results validates the simulation results and the introduced concept to build the RMTSs. The next phase of the measurement is accomplished by changing the angle between the receiver (fixed on the protractor arm) and the RMTS to determine the range of angles that are still viable to detect OAM beams, as a way to check the RMTSs sensitivity or misalignment cases. The protractor arm was varied with a step of $\pm 1°$ for a range of $\pm 10°$. By that, the receiver's location was varied for fixed transmitter and metasurface locations. Figs. 9(a), (b), and (c) confirms that the proposed RMTSs were capable of reflecting OAM beams for only $\pm 5°$ range of angles.

However, some scenarios may not require the continuous reshaping of the wireless transmission environment. An RMTS can be built to reconfigure the wireless propagation environment for specific scenarios to avoid
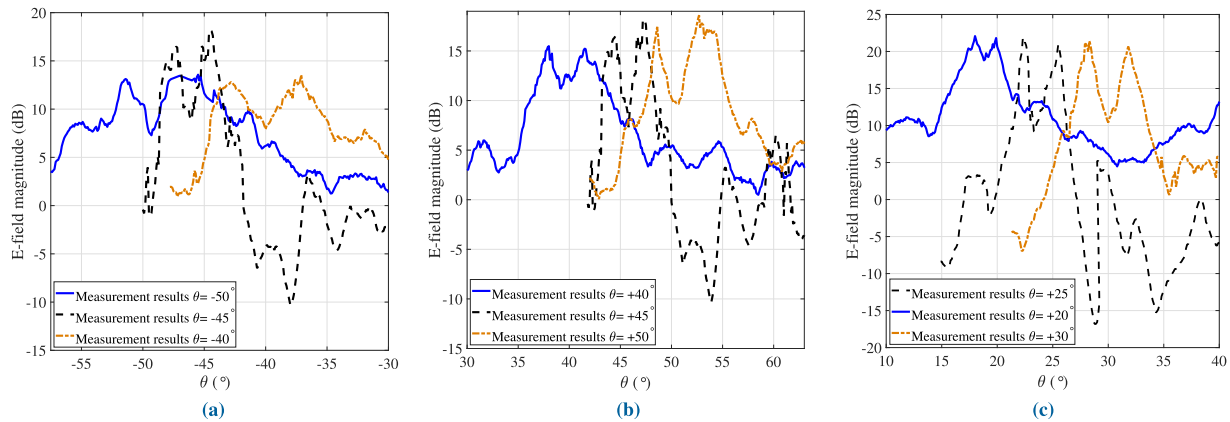
FIGURE 9. RMTSs sensitivity to the antenna misalignment at 90 GHz. (a) for $\theta = -50°$, $-45°$, and $-40°$, (b) for $\theta = 40°$, $45°$, and $50°$, (c) for $\theta = 20°$, $25°$, and $30°$.

blockage of the BSs links caused by obstacles. For this reason and to reduce the design's complexity, power consumption, and cost, multiple adjacent RMTSs can be employed without operating active elements. Thus, by directing different OAM beams towards the same receiver, OAM multiplexing can be achieved.

V. CONCLUSION

This paper proposed three reflective metasurfaces with single and dual directed OAM beams to tackle the poor network coverage of THz waves in the absence of LoS communications. The integration between the OAM and THz RMTS technologies can improve spectral efficiency through a low-cost and low-profile solution. The presented metasurfaces of 90×90 mm were simulated, fabricated, and tested to verify the capability to control and steer the wavefront of the EM waves at high frequencies. The discussed environment-friendly device can be a potential solution to be utilised for future wireless sixth-generation (6G) communications.

REFERENCES

[1] H. Sarieddeen, N. Saeed, T. Y. Al-Naffouri, and M.-S. Alouini, "Next generation terahertz communications: A rendezvous of sensing, imaging, and localization," *IEEE Commun. Mag.*, vol. 58, no. 5, pp. 69–75, May 2020.

[2] P. Hillger, J. Grzyb, R. Jain, and U. R. Pfeiffer, "Terahertz imaging and sensing applications with silicon-based technologies," *IEEE Trans. THz Sci. Technol.*, vol. 9, no. 1, pp. 1–19, Jan. 2019.

[3] O. Li, J. He, K. Zeng, Z. Yu, X. Du, Y. Liang, G. Wang, Y. Chen, P. Zhu, W. Tong, D. Lister, and L. Ibbotson, "Integrated sensing and communication in 6G a prototype of high resolution THz sensing on portable device," in *Proc. Joint Eur. Conf. Netw. Commun. 6G Summit (EuCNC/6G Summit)*, Jun. 2021, pp. 544–549.

[4] J. Ma, H. Liu, S.-Y. Zhang, W.-L. Zou, Y.-X. Fan, and Z.-Y. Tao, "Terahertz resonances of transverse standing waves in a corrugated plate waveguide," *IEEE Photon. J.*, vol. 14, no. 3, pp. 1–8, Jun. 2022.

[5] G.-B. Wu, K. F. Chan, and C. H. Chan, "3-D printed terahertz lens to generate higher order Bessel beams carrying OAM," *IEEE Trans. Antennas Propag.*, vol. 69, no. 6, pp. 3399–3408, Jun. 2021.

[6] K. Tsujimura, K. Umebayashi, J. Kokkoniemi, J. Lehtomaki, and Y. Suzuki, "A causal channel model for the terahertz band," *IEEE Trans. THz Sci. Technol.*, vol. 8, no. 1, pp. 52–62, Jan. 2018.

[7] G. B. Wu, K. F. Chan, S. W. Qu, K. F. Tong, and C. H. Chan, "Orbital angular momentum (OAM) mode-reconfigurable discrete dielectric lens operating at 300 GHz," *IEEE Trans. THz Sci. Technol.*, vol. 10, no. 5, pp. 480–489, Sep. 2020.

[8] A. Cagliero and R. Gaffoglio, "On the spectral efficiency limits of an OAM-based multiplexing scheme," *IEEE Antennas Wireless Propag. Lett.*, vol. 16, pp. 900–903, 2016.

[9] Y. Yuan, S. Sun, Y. Chen, K. Zhang, X. Ding, B. Ratni, Q. Wu, S. N. Burokur, and C. Qiu, "A fully phase-modulated metasurface as an energy-controllable circular polarization router," *Adv. Sci.*, vol. 7, no. 18, Sep. 2020, Art. no. 2001437, doi: 10.1002/advs.202001437.

[10] Z. Yang, Y. Hu, Z. Zhang, W. Xu, C. Zhong, and K.-K. Wong, "Reconfigurable intelligent surface based orbital angular momentum: Architecture, opportunities, and challenges," *IEEE Wireless Commun.*, vol. 28, no. 6, pp. 132–137, Dec. 2021.

[11] A. E. Willner, K. Pang, H. Song, K. Zou, and H. Zhou, "Orbital angular momentum of light for communications," *Appl. Phys. Rev.*, vol. 8, no. 4, Dec. 2021, Art. no. 041312, doi: 10.1063/5.0054885.

[12] R. Singh and D. C. Sicker, "THz communications—A boon and/or bane for security, privacy, and national security," *MatSciRN, Other Electron.*, to be published.

[13] Z. Chen, B. Ning, C. Han, Z. Tian, and S. Li, "Intelligent reflecting surface assisted terahertz communications toward 6G," *IEEE Wireless Commun.*, vol. 28, no. 6, pp. 110–117, Dec. 2021.

[14] M. Khalily, O. Yurduseven, T. J. Cui, Y. Hao, and G. V. Eleftheriades, "Engineered electromagnetic metasurfaces in wireless communications: Applications, research frontiers and future directions," *IEEE Commun. Mag.*, vol. 60, no. 10, pp. 88–94, Oct. 2022.

[15] Y. Wang, "Perfect control of diffraction patterns with phase-gradient metasurfaces," *ACS Appl. Mater. Interfaces*, vol. 14, no. 14, pp. 16856–16865, Apr. 2022, doi: 10.1021/acsami.2c00742.

[16] *Future Technology Trends of Terrestrial IMT Systems Towards 2030 and Beyond*, document R. I.-R. M.2516-0, Nov. 2022.

[17] Z. Chu, P. Xiao, D. Mi, W. Hao, M. Khalily, and L.-L. Yang, "A novel transmission policy for intelligent reflecting surface assisted wireless powered sensor networks," *IEEE J. Sel. Topics Signal Process.*, vol. 15, no. 5, pp. 1143–1158, Aug. 2021.

[18] M. Di Renzo, A. Zappone, M. Debbah, M.-S. Alouini, C. Yuen, J. de Rosny, and S. Tretyakov, "Smart radio environments empowered by reconfigurable intelligent surfaces: How it works, state of research, and the road ahead," *IEEE J. Sel. Areas Commun.*, vol. 38, no. 11, pp. 2450–2525, Nov. 2020.

[19] A. Araghi, "Reconfigurable intelligent surface (RIS) in the sub-6 GHz band: Design, implementation, and real-world demonstration," *IEEE Access*, vol. 10, pp. 2646–2655, 2022.

[20] D. Serghiou, M. Khalily, T. W. C. Brown, and R. Tafazolli, "Terahertz channel propagation phenomena, measurement techniques and modeling for 6G wireless communication applications: A survey, open challenges and future research directions," *IEEE Commun. Surveys Tuts.*, vol. 24, no. 4, pp. 1957–1996, 4th Quart., 2022.

[21] F. Qin, L. Wan, L. Li, H. Zhang, G. Wei, and S. Gao, "A transmission metasurface for generating OAM beams," *IEEE Antennas Wireless Propag. Lett.*, vol. 17, no. 10, pp. 1793–1796, Aug. 25, 2018.

[22] A. Ali, M. Khalily, T. Brown, and R. Tafazolli, "Beam-steering capability for OAM-based reflectarray at 5G-mmWave frequencies," *IET Microw., Antennas Propag.*, vol. 17, no. 2, pp. 162–168, Feb. 2023, doi: 10.1049/mia2.12333.

[23] A. Ali, M. Khalily, T. Brown, and R. Tafazolli, "Metasurface-based THz reflectarray antenna with vortex multiplexing and beam-steering capabilities for future wireless communications," *iScience*, vol. 25, no. 8, Aug. 2022, Art. no. 104725. [Online]. Available: https://www.sciencedirect.com/science/article/pii/S258900422200997X

[24] R. Chen, W.-X. Long, X. Wang, and L. Jiandong, "Multi-mode OAM radio waves: Generation, angle of arrival estimation and reception with UCAs," *IEEE Trans. Wireless Commun.*, vol. 19, no. 10, pp. 6932–6947, Oct. 2020.

[25] Z. Zhao, R. Zhang, H. Song, K. Pang, A. Almaiman, H. Zhou, H. Song, C. Liu, N. Hu, X. Su, A. Minoofar, H. Sasaki, D. Lee, M. Tur, A. F. Molisch, and A. E. Willner, "Modal coupling and crosstalk due to turbulence and divergence on free space THz links using multiple orbital angular momentum beams," *Sci. Rep.*, vol. 11, no. 1, p. 2110, Jan. 2021.

[26] G.-B. Wu, S.-W. Qu, C. Ma, S. Yang, and C. H. Chan, "Reflectarray antenna design with arbitrary incident and reflection beam angle," *IEEE Trans. Antennas Propag.*, vol. 66, no. 11, pp. 5964–5973, Nov. 2018.

[27] J. Shaker, M. Chaharmir, and J. Ethier, *Reflectarray Antennas: Analysis, Design, Fabrication, and Measurement* (Antennas and Propagation). Norwood, MA, USA: Artech House, 2013, pp. 25–45.

[28] H. Oraizi, A. Amini, A. Abdolali, and A. M. Karimimehr, "Design of wideband leaky-wave antenna using sinusoidally modulated impedance surface based on the holography theory," *IEEE Antennas Wireless Propag. Lett.*, vol. 17, no. 10, pp. 1807–1811, Oct. 2018.

[29] A. Ali, M. Khalily, A. Araghi, S. Hosseininejad, and R. Tafazolli, "OAM-based reflectarray antenna for THz indoor communications," in *Proc. IEEE Asia–Pacific Conf. Appl. Electromagn.*, Dec. 2021, pp. 1–4.

[30] A. Ali, M. Khalily, and R. Tafazolli, "Ultra-wideband dielectric reflectarray antenna with OAM beams for mm-wave applications," in *Proc. Int. Symp. Antennas Propag. (ISAP)*, Oct. 2022, pp. 381–382.

[31] K. Dovelos, S. D. Assimonis, H. Q. Ngo, B. Bellalta, and M. Matthaiou, "Intelligent reflecting surfaces at terahertz bands: Channel modeling and analysis," in *Proc. IEEE Int. Conf. Commun. Workshops (ICC Workshops)*, Jun. 2021, pp. 1–6.

[32] C.-H. Lee, S. W. Chi, J. Lee, and J. Lee, "Multi-beam transmitarray antenna design using principle of superposition," in *Proc. Int. Symp. Antennas Propag. (ISAP)*, Oct. 2018, pp. 1–2.

[33] Y. Li, X. Wan, B. Cai, Q. Cheng, and T. Cui, "Frequency-controls of electromagnetic multi-beam scanning by metasurfaces," *Sci. Rep.*, vol. 4, no. 1, p. 6921, Nov. 2014.

[34] C. Rusch, *Holographic Antennas*. Singapore: Springer, 2016, pp. 2689–2725, doi: 10.1007/978-981-4560-44-3_113.

[35] Y. Shi and Y. Zhang, "Generation of wideband tunable orbital angular momentum vortex waves using graphene metamaterial reflectarray," *IEEE Access*, vol. 6, pp. 5341–5347, 2017.

MOHSEN KHALILY (Senior Member, IEEE) is currently a Senior Lecturer (Associate Professor) in antennas and propagation and the Head of the Surface Electromagnetics Laboratory, Institute for Communication Systems, University of Surrey, U.K. He has published four book chapters and almost 200 academic articles in international peer-reviewed journals and conference proceedings. He has been the Principal Investigator on research grants totalling in excess of 1.6 million in the field of surface electromagnetics. His research interests include surface electromagnetics, electromagnetic engineered metasurfaces, phased arrays, THz metadevices, and mmWave and THz propagation.

He is a Delegate Member of the ETSI Industrial Specification Group on Reconfigurable Intelligent Surfaces and a fellow of the U.K. Higher Education Academy. He serves as an Associate Editor for the IEEE ANTENNAS AND WIRELESS PROPAGATION LETTERS, *Scientific Reports* (Nature), and IEEE ACCESS. He was the Lead Guest Editor in several journals, including IEEE ANTENNAS AND WIRELESS PROPAGATION LETTERS and IEEE OPEN JOURNAL OF ANTENNAS AND PROPAGATION, with the focus on metasurface engineering.

DEMOS SERGHIOU (Student Member, IEEE) received the M.E. degree in electrical and electronic engineering and the M.Sc. degree in antennas and propagation from the University of Surrey, Guildford, U.K., in 2018 and 2019, respectively, where he is currently pursuing the Ph.D. degree with the Institute of Communication Systems. His research interests include antenna design, propagation measurements, and modeling in the THz band.

RAHIM TAFAZOLLI (Senior Member, IEEE) has been a Professor of mobile and satellite communications, since April 2000. He has also been the Director of ICS, since January 2010, and the Founder and the Director of the 5G Innovation Centre, University of Surrey, U.K. He has more than 25 years of experience in digital communications research and teaching. He has authored or coauthored more than 500 research publications. He is a co-inventor of more than 30 granted patents, all in the field of digital communications.

In 2011, he was appointed as a fellow of the Wireless World Research Forum (WWRF) in recognition of his personal contributions to the wireless world and the heading one of Europe's leading research groups. He is regularly invited to deliver keynote talks and distinguished lectures to international conferences and workshops and many governments for advice on 5G Technologies. He was an Advisor to the Mayor of London with regard to the London Infrastructure Investment 2050 Plan, from May 2014 to June 2014. He has given many interviews to international media in the form of television, radio interviews, and articles in the international press.

ALI ALI (Graduate Student Member, IEEE) received the B.Sc. degree (Hons.) in electronic engineering and the M.Sc. degree (Hons.) in renewable energy and environmental engineering from Aleppo University, Aleppo, Syria, in 2014 and 2019, respectively. He is currently pursuing the Ph.D. degree in telecommunications engineering with the Home of 5G and 6G Innovation Centres, Institute for Communication Systems (ICS), University of Surrey, U.K.

His research interests include 5G-and-beyond networks, antenna design at mmWave and THz bands, metasurface, OAM beams, and satellite communications.